Int J Clin Exp Pathol 2018;11(5):2377-2388
www.ijcep.com /ISSN:1936-2625/IJCEP0075148

Original Article

Quantitative proteomic study of mitoxantrone-resistant NCI-H460 cell-xenograft tumors

Li Su[1], Shuang Cui[2], Hongying Zhen[3], Jiao Liu[1]

[1]*Center of Medical and Health Analysis,* [2]*Neuroscience Research Institute, Peking University, Beijing, China;* [3]*Department of Cell Biology, School of Basic Medical Sciences, Peking University Health Science Center, Beijing, China*

Received February 28, 2018; Accepted March 28, 2018; Epub May 1, 2018; Published May 15, 2018

Abstract: Mitoxantrone is one kind of chemical therapy medicine for cancer but certain kinds of cancer cells are chemical-resistant to it. In this research, we analyzed the quantitative proteomic difference between tumors *in vivo* xenograft by mitoxantrone-resistant (M group) and wild NCI-H460 cells (N group). Protein expression profiling in combination with pathway analysis was deployed to investigate molecular events associated with the tumors using a label-free quantitative proteomic approach. A total of 173 proteins were significantly differentially expressed in mitoxantrone-resistant tumors. Bioinformatics analysis using the cytoscape platform indicated that biological processes, including actin-mediated cell contraction, muscle system process, muscle filament sliding, and muscle contraction, are involved in mitoxantrone-resistance. As KEGG pathway enrichment analysis has shown, systemic lupus erythematosus, alcoholism, viral carcinogenesis, and tight junction are strongly regulated with chemical-resistance. By protein-protein interaction analysis, three protein clusters were found using k-means clustering algorithm. Dysregulation results can be verified by Western blotting. Further studies into the molecular functions of dysregulated proteins will help to provide new perspectives regarding chemoresistance for non-small cell lung cancers.

Keywords: Quantitative proteomics, bioinformatics, protein network, mitoxantrone, multi-drug resistance

Introduction

Lung cancer is the leading cause of cancer-related mortality worldwide, with a 5-year survival rate of only 18% [1]. The rate is still increasing. Non-small cell lung cancer (NSCLC) comprises 85-90% of lung cancer diagnoses [2], with 5-year survival < 20% [3, 4], especially large cell lung cancer. As one of the most important therapies, chemotherapy has not been as useful for large cell lung cancer compared with small cell lung cancer. The mechanism of resistance is not very clear.

Recent advances in analytical techniques present a new opportunity to examine the networks and offer a new view of pathologies and therapy targets. Proteomics is a collective study of all expressed proteins in cells, tissues, or biological fluids at a given time. It can reveal information not only on individual proteins but also their interplay in cellular components, biological processes, pathways, and special biochemical functions [5-7]. Liquid chromatography coupled with mass spectrometry (LC-MS) is a high-throughput experimental platform to measure thousands of proteins from complex biological samples, simultaneously [8]. Label-free quantitative proteomics can achieve a good balance between quantitative precision and number of quantified features [9]. It is reliable, versatile, and a cost-effective alternative compared to labeled quantitation [10].

There are many hypotheses to explain chemoresistance of cancers, such as cancer stem cells, micro-environments, etc. Detailed network perspective associated with mitoxantrone-resistance tumors remains unclear, however. In this research, we analyzed the proteomics of mitoxantrone-resistant and wild NCI-H460 cells xenografts tumors *in vivo* of female athymic nude mice (BALB/C). We also analyzed the bioinformatics and protein-protein interaction networks of dysregulated proteins. Detailed elucidations are as follows.

Materials and methods

3-(4,5-dimethylthiazol-2-yl)-5-(3-carboxymethoxyphenyl)-2-(4-sulfophenyl)-2H-tetrazolium (MTS), ammonium bicarbonate, sodium deoxycholate, and iodoacetamide were purchased from Sigma (St. Louis, MO, USA). Tris-(2-carboxyethyl) phosphine (TCEP) was acquired from Thermo Scientific (Rockford, Il, USA). Modified sequencing-grade trypsin was obtained from Promega (Madison, WI, USA). All mobile phases and solutions were prepared with HPLC grade solvents (i.e. water, acetonitrile, methanol, and formic acid) from Fisher. All other reagents were from commercial suppliers and of standard biochemical quality.

Cell lines and generation of chemoresistant cancer cells

Cancer cell line NCI-H460 was used. The chemotherapeutic drug mitoxantrone (MXR, 20 ng/mL) was used, a mutant from previous research [11]. In conclusion, the drug treatments were repeated twice or three times, mimicking the clinical regimen that patients with cancers would receive. This strategy ensured that more than 95% of cells underwent apoptosis or senescence with senescent cells eventually dying, thereby selecting the most resistant clones.

In vivo xenografts

Female athymic nude mice (BALB/C, 4-6 weeks of age) were used and all experimental procedures were performed according to protocols approved by the Peking University Health Science Center Animal Care and Use Committee. Each mouse was inoculated subcutaneously in both the side of flank with 5×10^6 H460 or H460/MTX cells suspended in 0.1 mL of serum-free medium containing 50% Matrigel (BD Biosciences, Bedford, MA). At 20 days after inoculation, all mice were sacrificed.

Protein preparation

After scarification, only 1 mm^3 of each tumor was used to prepare protein samples. In brief, they were grinded and ultrasonic oscillated in individual tubes. Tissue homogenates were lysed in RIPA buffer (Applygen, Beijing, China). After centrifugation (9000 rpm, 5 min, 4°C), supernatant of total proteins was removed to new tubes and protein concentration was determined by BCA assay (Pierce, Thermo Fisher Scientific, MA, USA). Each group was analyzed in triplicate.

Sample preparation for LC-MS

Protein samples (50 μg) from each group were processed, according to manufacturer protocol, for filter-aided sample preparation (FASP) [12]. Briefly, proteins were concentrated using Vivacon 500 filtration tubes (Cat No. VNO_1HO_2, Sartorius Stedim Biotech, UK), mixed with 100 μL of 8 M urea in 0.1 M Tris/HCL (pH 8.5) buffer, and centrifuged at 14,000 g and 4°C for 15 minutes. This step was performed twice, after which 10 μL of 0.05 M TCEP in water was added to the filters and samples were incubated at 37°C for 1 hour. Then, 10 μL of 0.1 M iodoacetamide (IAA) was added to the filters, afterwards the samples were incubated in darkness for 30 minutes. Filters were washed twice with 200 μL of 50 mM NH_4HCO_3. Finally, 1 μg of trypsin in 100 μL of 50 mM NH_4HCO_3 was added to each filter. The protein to enzyme ratio was 50:1. Samples were incubated overnight at 37°C and released peptides were collected by centrifugation.

LC-MS analysis

LC-MS experiments were performed on a nanoflow HPLC system (Easy-nLC 1000, Thermo Fisher Scientific, Waltham, MA, USA) connected to a Q-Exactive HF mass spectrometer (Thermo Fisher Scientific), equipped with a Nanospray Flex Ion Source (Thermo Fisher Scientific). One μg peptide mixtures (5 μL) were separated using a home-made reversed phase C18 column (75 μm I.D. × 20 mm, 3 μm particle size) at a flow rate of 300 nL/min. Chromatographic separation was performed with a 90 minute gradient of 2% to 40% acetonitrile in 0.1% formic acid. The electrospray voltage was maintained at 2.2 kV and capillary temperature was set at 275°C. Q-Exactive HF was operated in data-dependent mode to simultaneously measure full scan MS spectra (m/z 300-1800) in the Orbitrap with a mass resolution of 60,000 at m/z 400. After full-scan survey, the 20 most abundant ions detected in the full-MS scan were measured in the Orbitrap using HCD mode.

Protein identification and quantification

Data analysis was performed with MaxQuant software (version 1.6.0.16) (http://www.max-

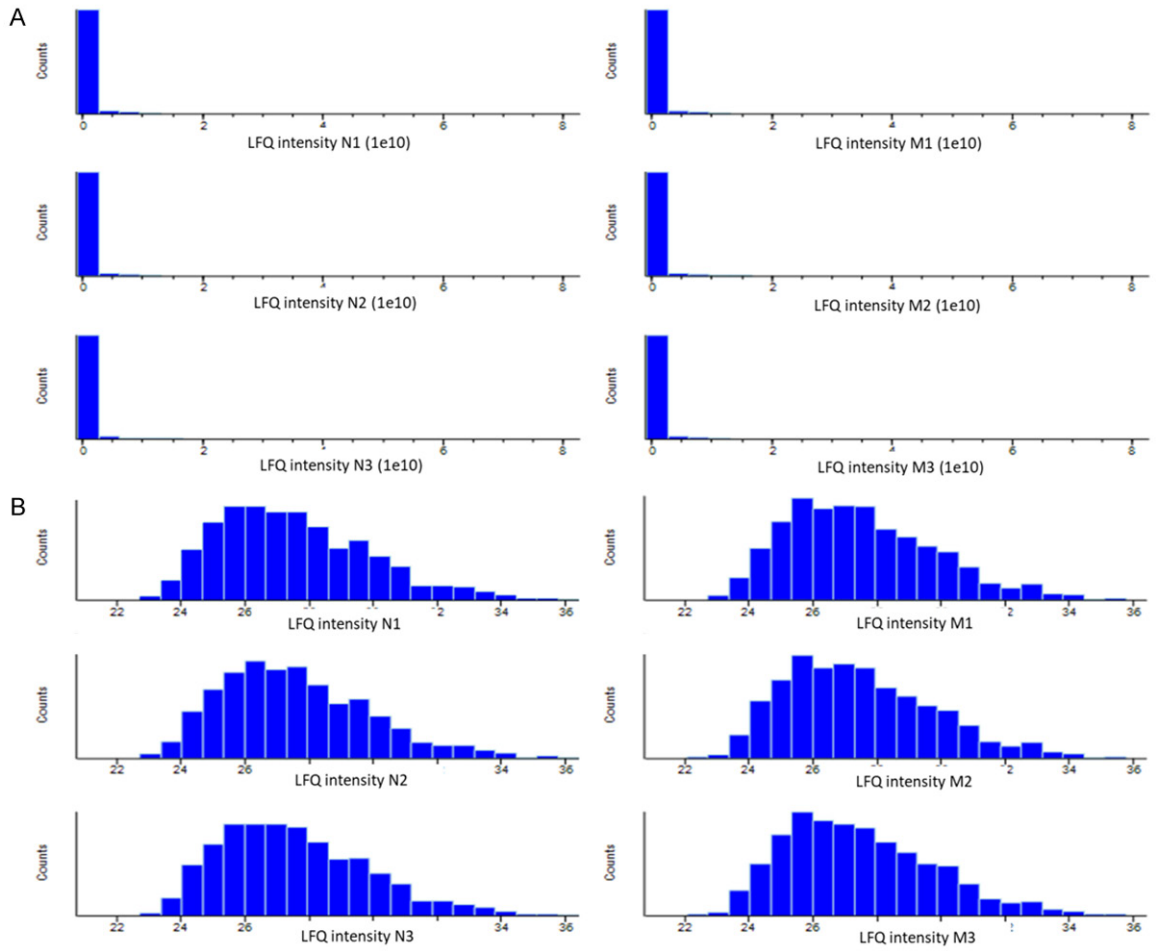

Figure 1. Histogram results of raw abundance of proteins before and after logarithm transformation. Histogram graph represents the protein expression distribution before (A) and after (B) logarithm (base 2) transformation. X-axis represents the intensities of proteins and Y-axis represents number of proteins. Protein expression shows a normal distribution pattern after log transformation.

quant.org/) [13]. For protein identification, MS/MS data were submitted to the Uniprot human protein database using the Andromeda search engine [14] with the following settings: trypsin cleavage; fixed modification of carbamidomethylation of cysteine; variable modifications of methionine oxidation; a maximum of two missed cleavages; false discovery rate of 0.01 at both peptide and protein level. Other parameters were set as default. These results were imported into Microsoft excel for further analysis. Label-free quantitation (LFQ) was also performed in MaxQuant. Minimum ratio count for LFQ was set to 2 and match-between-runs option was enabled. Other parameters were set as default. A 2-fold change in expression and a *p*-value of Student's t-test of 0.05 were used as a combined threshold to define biologically dysregulated proteins.

Bioinformatics analysis

Principal component analysis (PCA) and hierarchical clustering analysis were performed using MetaboAnalyst 3.0 web service (http://www.metaboanalyst.ca/). For bioinformatics analysis, the 172 differentially expressed proteins were used as inputs. Protein-protein interaction networks were constructed by STRING web service (http://www.string-db.org/). DAVID web service (https://david.ncifcrf.gov/) was used to retrieve the Gene Ontology Consortium (GOC, http://geneontology.org/) annotation results and KEGG pathway enrichment results.

Western blotting

The same protein samples for LC-MS analysis were also used for Western blotting assay. After

Table 1. Identification of differentially expressed proteins in mitoxantrone-resistant (M) and wild tumors NCI-H460 (N) cells xenografts tumors using LC-MS/MS

Majority Protein ID	Protein names	Gene names	Ratio (M/N)	-$\log_{10}$ *t*-test *p*-value
P09917	Arachidonate 5-lipoxygenase	ALOX5	0	6.21
E9PMR4	Tetraspanin	CD151	0	3.27
F8W8G8	Collagen alpha-5(VI) chain	COL6A5	0	3.72
P56537	Eukaryotic translation initiation factor 6	EIF6	0	4.55
Q8NEZ5	F-box only protein 22	FBXO22	0	3.68
Q9Y5Y0	Feline leukemia virus subgroup C receptor-related protein 1	FLVCR1	0	8.17
P09471	Guanine nucleotide-binding protein G(o) subunit alpha	GNAO1	0	5.44
P46734	Dual specificity mitogen-activated protein kinase kinase 3	MAP2K3	0	5.61
Q14696	LDLR chaperone MESD	MESDC2	0	5.49
Q96T76	MMS19 nucleotide excision repair protein homolog	MMS19	0	3.73
Q9UBG0	C-type mannose receptor 2	MRC2	0	3.09
Q86UY8	5-nucleotidase domain-containing protein 3	NT5DC3	0	4.65
Q96RS6	NudC domain-containing protein 1	NUDCD1	0	4.33
O95486	Protein transport protein Sec24A	SEC24A	0	3.69
B1AMS2	Septin-6	septin 6	0	4.84
Q9H936	Mitochondrial glutamate carrier 1	SLC25A22	0	5.45
J3KTL8	Structural maintenance of chromosomes flexible hinge domain-containing protein 1	SMCHD1	0	4.01
Q13813-3	Spectrin alpha chain, non-erythrocytic 1	SPTAN1	0	6.82
F8WF27	Transmembrane 4 L6 family member 1	TM4SF1	0	1.38
P67936	Tropomyosin alpha-4 chain	TPM4	0	4.02
Q99878	Histone H2A type 1-J	HIST1H2AJ	0.05	1.70
Q7LBC6	Lysine-specific demethylase 3B	KDM3B	0.18	1.71
P06396	Gelsolin	GSN	0.22	1.48
P20827	Ephrin-A1	EFNA1	0.22	1.55
P16402	Histone H1.3	HIST1H1D	0.23	2.09
D6RFM0	Ubiquitin-conjugating enzyme E2 D2	UBE2D2	0.23	1.50
P12532	Creatine kinase U-type, mitochondrial	CKMT1A	0.23	2.18
Q9C0B1	Alpha-ketoglutarate-dependent dioxygenase FTO	FTO	0.25	1.4
P11182	Lipoamide acyltransferase component of branched-chain alpha-keto acid dehydrogenase complex, mitochondrial	DBT	0.26	1.36
P16401	Histone H1.5	HIST1H1B	0.26	6.04
Q9H0E9	Bromodomain-containing protein 8	BRD8	0.26	1.96
P10124	Serglycin	SRGN	0.27	4.09
K7EKP1	Apolipoprotein C-I	APOC1	0.30	1.54
E7EQB2	Lactotransferrin	LTF	0.33	2.60
P16403	Histone H1.2	HIST1H1C	0.36	2.88
Q71UI9	Histone H2A.V	H2AFV	0.36	1.79
Q16778	Histone H2B type 2-E	HIST2H2BE	0.37	1.45
A8MYE6	Integrin beta	ITGB2	0.39	3.69
P11215	Integrin alpha-M	ITGAM	0.41	3.8
P01008	Antithrombin-III	SERPINC1	0.41	4.00
P98088	Mucin-5AC	MUC5AC	0.41	6.71
Q5TEC6	Histone H3	HIST2H3PS2	0.43	1.52
P12955	Xaa-Pro dipeptidase	PEPD	0.44	4.40
P05164	Myeloperoxidase	MPO	0.45	6.02
B4DR52	Histone H2B	HIST1H2BN	0.46	3.99
O75531	Barrier-to-autointegration factor	BANF1	0.47	1.52
P62805	Histone H4	HIST1H4A	0.47	4.19

P00352	Retinal dehydrogenase 1	ALDH1A1	0.47	4.62
Q6FI13	Histone H2A type 2-A	HIST2H2AA3	0.47	3.77
P05204	Non-histone chromosomal protein HMG-17	HMGN2	0.48	2.65
P00747	Plasminogen	PLG	0.48	2.73
E9PBJ0	Mucin-5B	MUC5B	0.49	5.83
Q01081	Splicing factor U2AF 35 kDa subunit	U2AF1	2.03	3.68
P22087	rRNA 2-O-methyltransferase fibrillarin	FBL	2.04	6.04
A6NN80	Annexin A6	ANXA6	2.05	6.17
O00499	Myc box-dependent-interacting protein 1	BIN1	2.09	1.78
F5H7V9	Tenascin	TNC	2.11	4.36
P04264	Keratin, type II cytoskeletal 1	KRT1	2.19	4.25
Q8NI27	THO complex subunit 2	THOC2	2.25	1.90
Q9UBR2	Cathepsin Z	CTSZ	2.35	4.63
Q96PZ0	Pseudouridylate synthase 7 homolog	PUS7	2.46	1.32
P50402	Emerin	EMD	2.48	1.32
F5H6U7	Vesicle transport protein GOT1B	GOLT1B	2.63	1.93
Q96FQ6	Protein S100-A16	S100A16	2.67	4.29
Q13642	Four and a half LIM domains protein 1	FHL1	2.82	2.89
P60903	Protein S100-A10	S100A10	2.96	4.09
P68133	Actin, alpha skeletal muscle	ACTA1	3.42	4.73
P11217	Glycogen phosphorylase, muscle form	PYGM	3.58	4.01
P41223	Protein BUD31 homolog	BUD31	3.92	1.32
Q8NBW7	ER lumen protein-retaining receptor 1	KDELR1	3.95	2.18
P23786	Carnitine O-palmitoyltransferase 2, mitochondrial	CPT2	4.00	1.33
Q8N0U8	Vitamin K epoxide reductase complex subunit 1-like protein 1	VKORC1L1	4.01	1.40
P50238	Cysteine-rich protein 1	CRIP1	4.06	1.42
Q7Z4H3	HD domain-containing protein 2	HDDC2	4.10	1.34
Q9H2W6	39S ribosomal protein L46, mitochondrial	MRPL46	4.29	1.35
P14618	Pyruvate kinase PKM	PKM; PKM2	4.31	1.46
Q9NVP1	ATP-dependent RNA helicase DDX18	DDX18	4.44	1.58
P98160	Basement membrane-specific heparan sulfate proteoglycan core protein	HSPG2	4.54	1.60
Q8IYB8	ATP-dependent RNA helicase SUPV3L1, mitochondrial	SUPV3L1	4.54	1.51
O00139	Kinesin-like protein KIF2A	KIF2A	4.61	1.53
O00767	Acyl-CoA desaturase	SCD	4.86	1.73
Q86UX7	Fermitin family homolog 3	FERMT3	5.00	1.69
F5H4G7	Importin subunit alpha-6	KPNA6	5.01	1.72
B4E0V0	Pyridoxine-5-phosphate oxidase	PNPO	6.44	2.03
Q86TD4	Sarcalumenin	SRL	8.12	2.67
P07451	Carbonic anhydrase 3	CA3	9.19	5.59
E9PR30	40S ribosomal protein S30	FAU	25.28	4.61
P12882	Myosin-1	MYH1	34.78	5.65
P13929	Beta-enolase	ENO3	40.44	2.95
P06732	Creatine kinase M-type	CKM	140.97	3.70
F5GYC1	ATP-binding cassette sub-family D member 3	ABCD3	#DIV/0!	4.67
P35609	Alpha-actinin-2	ACTN2	#DIV/0!	3.46
Q9UKV8	Protein argonaute-2	AGO2	#DIV/0!	3.30
Q9BT22	Chitobiosyldiphosphodolichol beta-mannosyltransferase	ALG1	#DIV/0!	3.85
Q5VY93	Rho guanine nucleotide exchange factor 2	ARHGEF2	#DIV/0!	3.01
Q96BM9	ADP-ribosylation factor-like protein 8A	ARL8A	#DIV/0!	6.74
O14983	Sarcoplasmic/endoplasmic reticulum calcium ATPase 1	ATP2A1	#DIV/0!	4.43
Q93084	Sarcoplasmic/endoplasmic reticulum calcium ATPase 3	ATP2A3	#DIV/0!	4.26
P46100	Transcriptional regulator ATRX	ATRX	#DIV/0!	5.97
C9JGJ9	B-cell receptor-associated protein 29	BCAP29	#DIV/0!	4.71

O75934	Pre-mRNA-splicing factor SPF27	BCAS2	#DIV/0!	3.05
P46736	Lys-63-specific deubiquitinase BRCC36	BRCC3	#DIV/0!	3.00
F5GX99	Caseinolytic peptidase B protein homolog	CLPB	#DIV/0!	5.06
P09497	Clathrin light chain B	CLTB	#DIV/0!	6.07
A6NLH6	Protein cornichon homolog 4	CNIH4	#DIV/0!	6.35
E9PJL7	Alpha-crystallin B chain	CRYAB	#DIV/0!	3.11
Q13363	C-terminal-binding protein 1	CTBP1	#DIV/0!	2.08
P07858	Cathepsin B	CTSB	#DIV/0!	6.02
Q9BVQ8	Probable ATP-dependent RNA helicase DDX49	DDX49	#DIV/0!	2.81
P00374	Dihydrofolate reductase	DHFR	#DIV/0!	5.94
Q8IYJ9	Dual specificity protein phosphatase 3	DUSP3	#DIV/0!	3.78
P49770	Translation initiation factor eIF-2B subunit beta	EIF2B2	#DIV/0!	4.70
P11171	Protein 4.1	EPB41	#DIV/0!	3.36
C9JAG1	Ethanolaminephosphotransferase 1	EPT1	#DIV/0!	4.80
Q14315	Filamin-C	FLNC	#DIV/0!	7.06
A8MQB8	Fragile X mental retardation protein 1	FMR1	#DIV/0!	3.83
Q14C86	GTPase-activating protein and VPS9 domain-containing protein 1	GAPVD1	#DIV/0!	5.79
O00461	Golgi integral membrane protein 4	GOLIM4	#DIV/0!	2.86
B7WNW7	HEAT repeat-containing protein 3	HEATR3	#DIV/0!	5.08
O43719	HIV Tat-specific factor 1	HTATSF1	#DIV/0!	3.71
O15357	Phosphatidylinositol 3,4,5-trisphosphate 5-phosphatase 2	INPPL1	#DIV/0!	4.52
Q68E01	Integrator complex subunit 3	INTS3	#DIV/0!	4.29
Q14573	Inositol 1,4,5-trisphosphate receptor type 3	ITPR3	#DIV/0!	3.70
H0Y8E4	Kinase D-interacting substrate of 220 kDa	KIDINS220	#DIV/0!	3.38
O75112	LIM domain-binding protein 3	LDB3	#DIV/0!	5.79
P21397	Amine oxidase [flavin-containing] A	MAOA	#DIV/0!	4.94
Q9P015	39S ribosomal protein L15, mitochondrial	MRPL15	#DIV/0!	5.32
Q96DV4	39S ribosomal protein L38, mitochondrial	MRPL38	#DIV/0!	3.92
Q13405	39S ribosomal protein L49, mitochondrial	MRPL49	#DIV/0!	6.04
B8ZZU9	Bifunctional methylenetetrahydrofolate dehydrogenase/cyclohydrolase, mitochondrialdehydrogenase	MTHFD2	#DIV/0!	4.31
Q14324	Myosin-binding protein C, fast-type	MYBPC2	#DIV/0!	3.66
Q9UKX2	Myosin-2	MYH2	#DIV/0!	6.62
Q9Y623	Myosin-4	MYH4	#DIV/0!	2.50
P12883	Myosin-7	MYH7	#DIV/0!	3.79
Q96A32	Myosin regulatory light chain 2, skeletal muscle isoform	MYLPF	#DIV/0!	3.06
S4R3I5	NADH dehydrogenase [ubiquinone] 1 alpha subcomplex subunit 3	NDUFA3	#DIV/0!	3.63
H0Y9M8	NADH dehydrogenase [ubiquinone] iron-sulfur protein 4, mitochondrial	NDUFS4	#DIV/0!	5.69
C9J808	MKI67 FHA domain-interacting nucleolar phosphoprotein	NIFK	#DIV/0!	5.67
P46087	Probable 28S rRNA (cytosine(4447)-C(5))-methyltransferase	NOP2	#DIV/0!	4.01
Q5TFE4	5-nucleotidase domain-containing protein 1	NT5DC1	#DIV/0!	5.57
Q9NPF4	Probable tRNA N6-adenosine threonylcarbamoyltransferase	OSGEP	#DIV/0!	3.74
J3KNQ4	Alpha-parvin	PARVA	#DIV/0!	5.65
Q15118	[Pyruvate dehydrogenase (acetyl-transferring)] kinase isozyme 1, mitochondrial	PDK1	#DIV/0!	3.54
P15259	Phosphoglycerate mutase 2	PGAM2	#DIV/0!	2.44
Q969N2	GPI transamidase component PIG-T	PIGT	#DIV/0!	4.81
P24928	DNA-directed RNA polymerase II subunit RPB1	POLR2A	#DIV/0!	4.36
E9PG73	Peptidyl-prolyl cis-trans isomerase G	PPIG	#DIV/0!	4.12
P50336	Protoporphyrinogen oxidase	PPOX	#DIV/0!	4.02
P51888	Prolargin	PRELP	#DIV/0!	3.10
P17252	Protein kinase C alpha type	PRKCA	#DIV/0!	5.20
A2A2V1	Major prion protein	PRNP	#DIV/0!	4.91
E7EVX8	U4/U6 small nuclear ribonucleoprotein Prp31	PRPF31	#DIV/0!	4.24

O95758	Polypyrimidine tract-binding protein 3	PTBP3	#DIV/0!	3.83
Q92878	DNA repair protein RAD50	RAD50	#DIV/0!	6.15
H0YAE9	Ribonuclease T2	RNASET2	#DIV/0!	4.24
D6RD69	GTP-binding protein SAR1b	SAR1B	#DIV/0!	5.07
Q86TU7	Histone-lysine N-methyltransferase setd3	SETD3	#DIV/0!	5.76
O15374-4	Monocarboxylate transporter 5	SLC16A4	#DIV/0!	4.55
O00186	Syntaxin-binding protein 3	STXBP3	#DIV/0!	4.09
E7EMB1	Switch-associated protein 70	SWAP70	#DIV/0!	2.97
P57105	Synaptojanin-2-binding protein	SYNJ2BP	#DIV/0!	2.64
E9PF19	Transducin beta-like protein 2	TBL2	#DIV/0!	4.88
Q92544	Transmembrane 9 superfamily member 4	TM9SF4	#DIV/0!	5.47
P02585	Troponin C, skeletal muscle	TNNC2	#DIV/0!	7.89
P48788	Troponin I, fast skeletal muscle	TNNI2	#DIV/0!	3.21
H9KVA2	Troponin T, fast skeletal muscle	TNNT3	#DIV/0!	3.65
Q8NFQ8	Torsin-1A-interacting protein 2	TOR1AIP2	#DIV/0!	3.40
Q6ZMU5	Tripartite motif-containing protein 72	TRIM72	#DIV/0!	3.69
B4DEB8	Tetraspanin-7	TSPAN7	#DIV/0!	4.35
Q6PGP7	Tetratricopeptide repeat protein 37	TTC37	#DIV/0!	2.32
Q9BZX2	Uridine-cytidine kinase 2	UCK2	#DIV/0!	3.72
Q5MNZ6	WD repeat domain phosphoinositide-interacting protein 3	WDR45B	#DIV/0!	3.56
Q5BJH7	Protein YIF1B	YIF1B	#DIV/0!	4.52

the addition of sample loading buffer, protein samples of each group were separated using 10% SDS-PAGE and subsequently transferred to PVDF membrane (Millipore). The membrane was incubated in fresh blocking buffer (0.1% Tween 20 in Tris-buffered saline, pH 7.4, containing 5% non-fat dried milk) at room temperature for 1 hour and then probed with monoclonal mouse anti-RAD50 antibody (Abcam, Cambridge, UK) and mouse anti-glyceraldehyde-3-phosphate dehydrogenase (GAPDH) antibody (Zhongshan Gold Bridge Biotechnology Co. Ltd, China) in blocking buffer at 4°C overnight. Membranes were washed three times for 5 minutes each using PBST (PBS containing 0.1% Tween-20), then incubated with appropriate horseradish peroxidase (HRP)-conjugated secondary antibody at room temperature for 1 hour. Then, it was washed three more times in PBST buffer. The membrane was finally incubated with ECL substrate solution (ECL Kit, Perkinelmer) for 5 minutes, according to manufacturer instructions, and visualized with autoradiographic film.

Statistical analysis

Results are expressed as mean ± S.E.M. Statistical evaluation was performed using Student's t-test (for comparing two value sets). $P < 0.05$ was considered statistically significant (*$P < 0.05$: **$P < 0.01$).

Results

Many proteins expressed different degrees between two kinds of tumors

From histogram results of raw abundance of proteins before and after logarithm transformation, as shown in **Figure 1**, protein expression revealed a normal distribution pattern after log transformation confirming the reliability of proteomics analysis. Statistical analysis with Perseus software was performed to select proteins that were differentially expressed between two kinds of tumors, using the following criteria: fold change > 2 or < 0.5, *p*-value < 0.01 (using Student's t-test). Among thousands of proteins, there were 173 proteins dysregulated between the two kinds of tumors (**Table 1**). 52 proteins were downregulated in the M groups, during which there were twenty proteins only detected in the N groups. The other 121 proteins were highly upregulated and 83 of them only detected in the M groups.

An overview of proteomics analysis of the tumors is shown in **Figure 2A**, a PCA score plot of the two groups in terms of PC1 (X-axis) and PC2 (Y-axis). The two groups are presented by red (group N) and green (group M). **Figure 2B** shows volcano plot of the 2,406 proteins quantified. We determined the fold change in protein expression as X-axis represents fold change

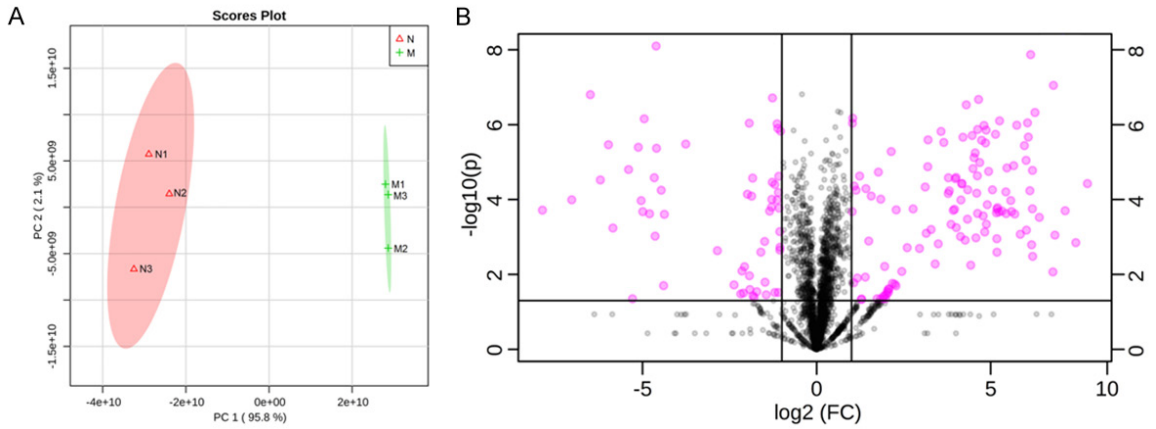

Figure 2. Overview of proteomic analysis of the tumors. A: PCA score plot of the two groups in terms of PC1 (X-axis) and PC2 (Y-axis). The two groups are presented by red (group B) and green (group LA). B: Volcano plot of the 2,406 proteins quantified. X-axis represents fold change (group M/N), and Y-axis represents -log10 (*p*-value). Up- and down-regulated proteins are colored pink.

(group M/N) and Y-axis represents log10 (*p*-value). Up- and down-regulated proteins are colored in pink. Expression levels of the 172 proteins in all samples are shown in the heat map generated by hierarchical cluster analysis, displaying a clear difference in mitoxantrone-resistant (M) and wild NCI-H460 (N) cell xenograft tumors (**Figure 3A**).

Bioinformatics analysis

To better understand the regulative network influenced by treatment, we analyzed the expression pattern and bioinformatics analysis of significantly dysregulated proteins using dysregulated proteins as inputs. **Figure 3B** shows the top 14 items of gene ontology enrichment analysis in terms of cellular components. X-axis represents -log10 (*p*-value). The cellular locations of these dysregulated proteins were mainly at sarcomere, contractile fiber part, contractile fiber, myofibril, and organelle part et al. **Figure 3C** shows the top 14 items of gene ontology enrichment analysis in terms of biological processes. Dysregulated proteins influenced by treatment were related with several biological processes. Bioinformatics analysis, using the cytoscape platform, indicated that biological processes, including actin-mediated cell contraction, muscle system process, muscle filament sliding, and muscle contraction, are involved in mitoxantrone-resistance. **Figure 3D** shows the top 14 items of gene ontology enrichment analysis in terms of molecular function. Their functions were included in binding, anion binding, carbohydrate derivative binding, small molecule binding, and structural molecule activity et al. As KEGG pathway enrichment analysis shows in **Figure 3E**, systemic lupus erythematosus, alcoholism, viral carcinogenesis, and tight junction were strongly regulated with mitoxantrone-resistance.

To construct a protein-protein interaction network associated with two kinds of tumors, we matched the 173 significantly differently expressed proteins with regulatory and data protein-protein interaction networks were constructed by STRING web service (http://www.string-db.org/) (**Figure 4**). Each node represents a protein and each line represents one kind of known interaction. Three protein clusters were found, using k-means clustering algorithm, and are represented by different node colors (green, red, and blue).

Western blot verification of differentially expressed protein RAD50

RAD 50 is one of the important proteins dysregulated between the two groups. We verified its different expression by Western blot and got the same conclusion of its upregulation in the mitoxantrone-resistant cell xenografts group (**Figure 5**).

Discussion

Tumor cell xenografts in athymic nude mice are popular models for cancer research. Animal models enable us to further understand molecular and regulatory mechanisms of tumors

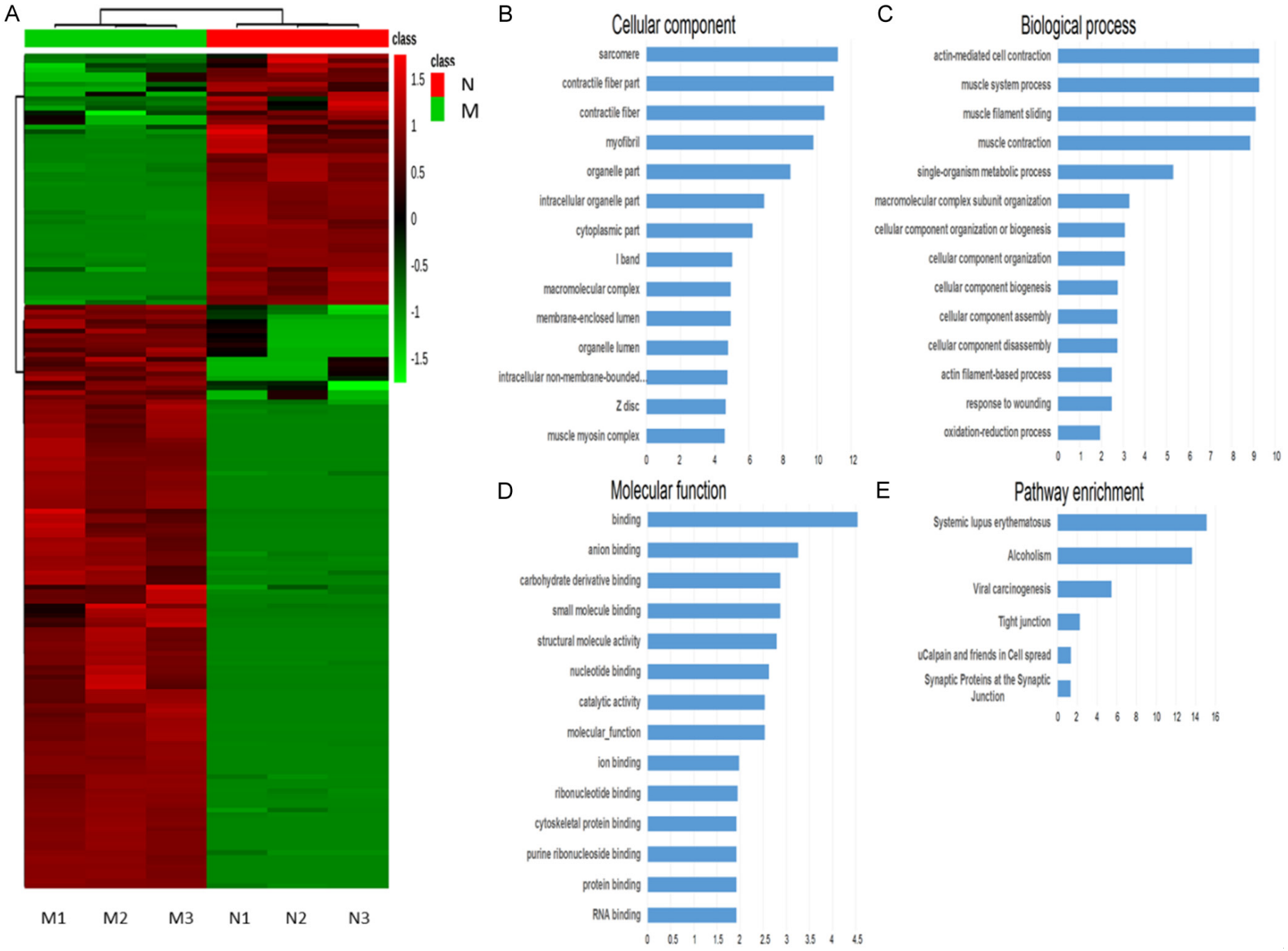

Figure 3. Expression pattern and bioinformatics analysis of significantly dysregulated proteins. A: Heat map representing the hierarchical clustering analysis results of the dysregulated proteins. Red represents upregulated proteins in group M and green represents downregulated proteins. B: Top 15 items of the gene ontology enrichment analysis in terms of cellular component. X-axis represents -log10 (*p*-value). C: Top 15 items of the gene ontology enrichment analysis in terms of biological process. D: Top 15 items of the gene ontology enrichment analysis in terms of molecular function. E: KEGG pathway enrichment analysis.

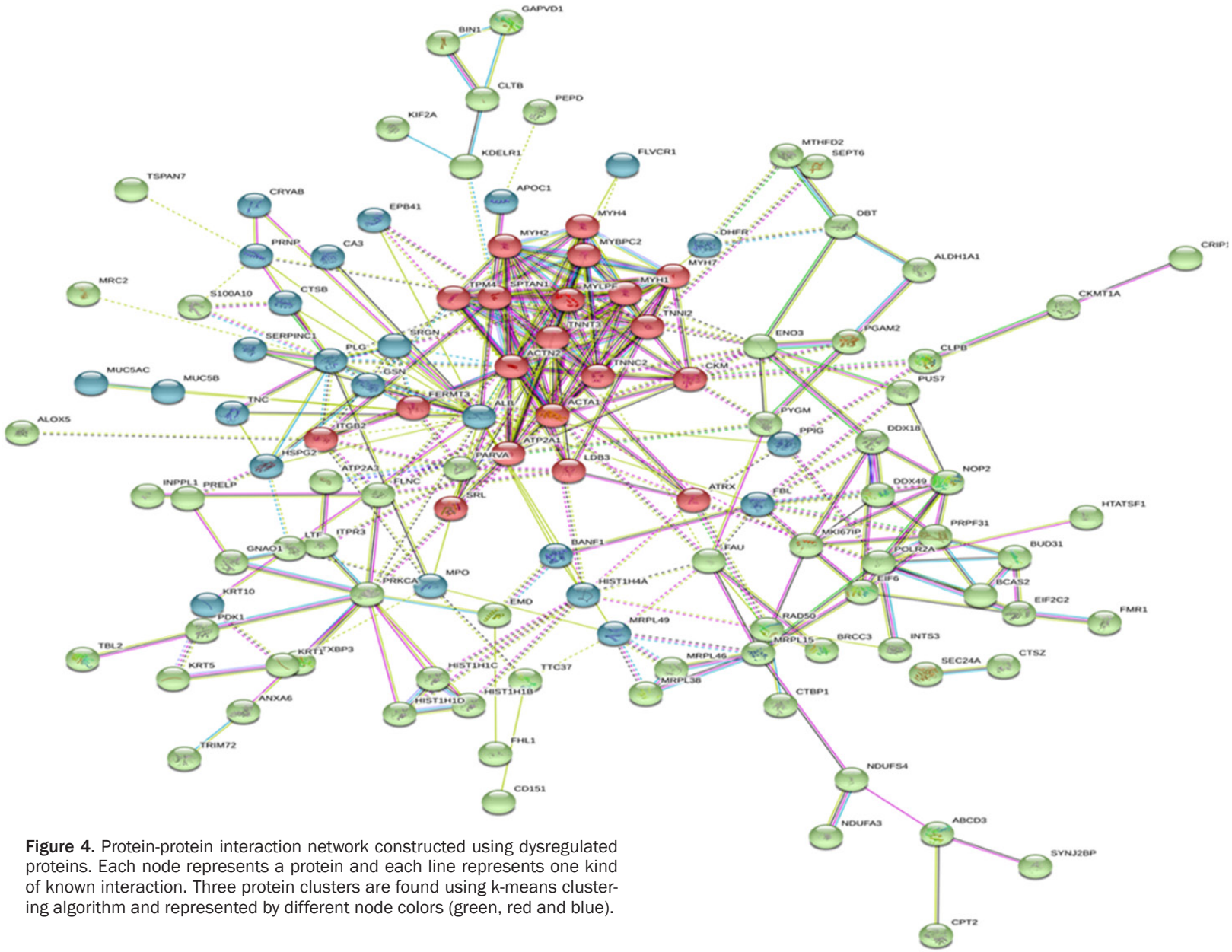

Figure 4. Protein-protein interaction network constructed using dysregulated proteins. Each node represents a protein and each line represents one kind of known interaction. Three protein clusters are found using k-means clustering algorithm and represented by different node colors (green, red and blue).

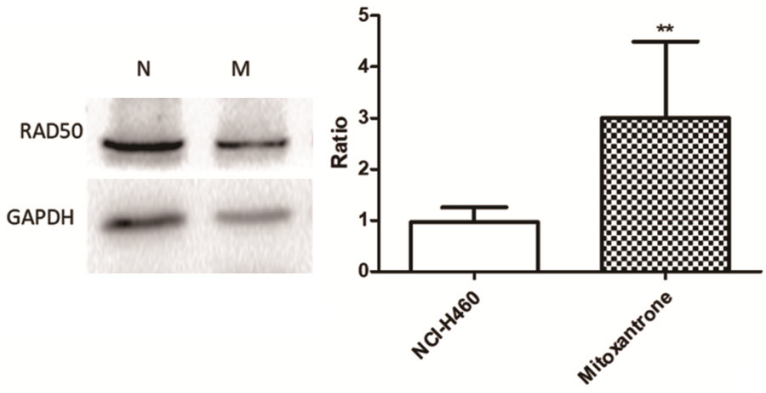

Figure 5. Western blotting of RAD50 expression *in vivo* xenograft tumors. The band intensity shows that mitoxantrone-resistant cells xenograft results in upregulation of RAD50 compared with wild NCI-H460 cells xenograft. Data are means ± SD of the results from three independent experiments, **P < 0.01.

such as occurrence, development, and multidrug resistance (MDR). Compared with cellular studies *in vitro*, animal models of MDR have more clinical value. Chemoresistant cell xenografts are usually used as MDR models *in vivo* [15, 16]. NCI-H460 is a kind of non-small cell lung cancer (NSCLC) cell line and the mitoxantrone-resistance cell line is usually used for MDR mechanism *in vitro*. Deep research on mitoxantrone-resistance cell xenografts will be very helpful in understanding the MDR mechanism of NSCLC.

High throughput proteomics by liquid chromatography mass spectrometry (LC-MS) has become core instrumentation offering highly relevant information towards biology including protein composition, post-translational modifications, and protein dynamics, due to its performance and sensitivity [17, 18]. Using network analysis, bioinformatic analysis of pathway levels and protein-protein interaction is popular and helpful for biological and medicine research such as diagnosing disease phenotype by identification of disease-specific biomarkers for cancer [19], neurodegeneration diagnosis [20], and other diseases [21]. For example, Diederick discovered novel biomarkers for prostate cancer progression using LC-MS mode [22]. Therefore, it is a powerful tool for connecting genotypes to phenotypes.

Bioinformatics is a useful tool for analyzing high throughput data from genomics, proteomics, metabolomics, and lipidomics [23]. There are many kinds of databases online, such as DIP, BIND, Intact, KEGG, and STRING. Each of them can provide different protein-protein interaction information on metabolic and signaling pathways or multiple organisms. All of these can provide useful and important information in understanding complex pathogeneses or biological phenomena. In this research, we identified 173 dysregulated proteins between tumors forming from mitoxantrone-resistant and wild NCI-H460 cell xenografts. Bioinformatics analysis showed that they belong to three protein-protein interaction clusters and all of them can interact by weak or hard connections. There are some important proteins which lie in the cores and connect to other proteins, including Rad 50. Rad 50 is involved in many biological processes including single-organism metabolic process, cellular component organization, cellular component organization or biogenesis, and response to stress. It can detect damage both of nuclear DNA and virus DNA and then induce immune responses [24]. We also verified upregulation of Rad50 in mitoxantrone-resistant tumors by Western blot analysis, demonstrating the reliability of proteomics results. Nevertheless, there are so many different proteins that clear function researches are needed to attain a deep understanding of chemoresistant mechanisms of cancer therapies. These will also be helpful in finding new targets for clinical therapies.

Acknowledgements

This work was partly supported by the National Natural Science Foundation of China (30700206, 31700898).

Disclosure of conflict of interest

None.

Address correspondence to: Drs. Li Su and Jiao Liu, Center of Medical and Health Analysis, Peking University, 38 Xueyuan Road, Haidian District, Beijing 100191, China. Tel: +86-10-8280-5034; Fax: +86-10-8280-5034; E-mail: dudu.su@163.com (LS); Tel: +86-10-8280-2389; E-mail: 15120087-482@163.com (JL)

References

[1] Siegel RL, Miller KD, Jemal A. Cancer statistics. CA Cancer J Clin 2017; 67: 7-30.

[2] Kanaan Z, Kloecker GH, Paintal A, Perez CA. Novel targeted therapies for resistant ALK-rearranged non-small-cell lung cancer: ceritinib and beyond. Onco Targets Ther 2015; 8: 885-892.

[3] Mostafa AA, Morris DG. Immunotherapy for lung cancer: has it finally arrived? Front Oncol 2014; 4: 288.

[4] Jung MJ, Rho JK, Kim YM, Jung JE, Jin YB, Ko YG, Lee JS, Lee SJ, Lee JC, Park MJ. Upregulation of CXCR4 is functionally crucial for maintenance of stemness in drug-resistant non-small cell lung cancer cells. Oncogene 2013; 32: 209-221.

[5] Wasinger VC, Cordwell SJ, Cerpa-Poljak A, Yan JX, Gooley AA, Wilkins MR, Duncan MW, Harris R, Williams KL, Humphery-Smith I. Progress with gene-product mapping of the Mollicutes: mycoplasma genitalium. Electrophoresis 1995; 6: 1090-1094.

[6] Wilkins MR, Sanchez JC, Gooley AA, Appel RD, Humphery-Smith I, Hochstrasser DF, Williams KL. Progress with proteome projects: why all proteins expressed by a genome should be identified and how to do it. Biotechnol Genet Eng Rev 1996; 13: 19-50.

[7] Walther TC, Mann M. Mass spectrometry-based proteomics in cell biology. J Cell Biol 2010; 190: 491-500.

[8] Ong SE, Mann M. Mass spectrometry-based proteomics turns quantitative. Nat Chem Biol 2005; 1: 252-262.

[9] Liu NQ, Dekker LJ, Sting IC, Güzel C, De Marchi T, Martens JW, Foekens JA, Luider TM, Umar A. Quantitative proteomic analysis of microdissected breast cancer tissues: comparison of label-free and SILAC-based quantification with shotgun, directed, and targeted MS approaches. J Proteome Res 2013; 12: 4627-4641.

[10] Neilson KA, Ali NA, Muralidharan S, Mirzaei M, Mariani M, Assadourian G, Lee A, van Sluyter SC, Haynes PA. Less label, more free: approaches in label-free quantitative mass spectrometry. Proteomics 2011; 11: 535-553.

[11] Wang XQ, Ongkeko WM, Chen L, Yang ZF, Lu P, Chen KK, Lopez JP, Poon RT, Fan ST. Octamer 4 (Oct4) mediates chemotherapeutic drug resistance in liver cancer cells through a potential Oct4-AKT-ATP-binding cassette G2 pathway. Hepatology 2010; 52: 528-539.

[12] Wisniewski JR, Zougman A, Nagaraj N, Mann M. Universal sample preparation method for proteome analysis. Nat Methods 2009; 6: 359-362.

[13] Cox J, Mann M. MaxQuant enables high peptide identification rates, individualized p.p.b.-range mass accuracies and proteome-wide protein quantification. Nat Biotechnol 2008; 26: 1367-1372.

[14] Cox J, Neuhauser N, Michalski A, Scheltema RA, Olsen JV, Mann M. Andromeda: a peptide search engine integrated into the MaxQuant environment. J Proteome Res 2011; 10: 1794-1805.

[15] Zhang W, Chen Z, Chen LK, Wang F, Li FR, Wang XK, Fu LW. ABCG2-overexpressing H460/MX20 cell xenografts in athymic nude mice maintained original biochemical and cytological characteristics. Sci Rep 2017; 7: 40064.

[16] Chao TT, Wang CY, Chen YL, Lai CC, Chang FY1, Tsai YT, Chao CH, Shiau CW, Huang YC, Yu CJ, Chen KF. Afatinib induces apoptosis in NSCLC without EGFR mutation through Elk-1-mediated suppression of CIP2A. Oncotarget 2015; 6: 2164-2179.

[17] Lesley SA. High-throughput proteomics: protein expression and purification in the postgenomic world. Protein Expr Purif 2001; 22: 159-164.

[18] Rodriguez-Aller M, Gurny R, Veuthey JL, Guillarme D. Coupling ultra high-pressure liquid chromatography with mass spectrometry: constraints and possible applications. J Chromatogr A 2013; 1292: 2-18.

[19] Srinivas PR, Srivastava S, Hanash S Jr, Wright GL. Proteomics in early detection of cancer. Clin Chem 2001; 47: 1901-1911.

[20] Liguori M, Qualtieri A, Tortorella C, Direnzo V, Bagala A, Mastrapasqua M, Spadafora P, Trojano M. Proteomic profiling in multiple sclerosis clinical courses reveals potential biomarkers of neurodegeneration. PLoS One 2014; 9: e103984.

[21] Télot L, Rousseau E, Lesuisse E, Garcia C, Morlet B, Léger T, Camadro JM, Serre V. Quantitative proteomics in Friedreich's ataxia B-lymphocytes: a valuable approach to decipher the biochemical events responsible for pathogenesis. Biochim Biophys Acta 2018; 1864: 997-1009.

[22] Duijvesz D, Burnum-Johnson KE, Gritsenko MA, Hoogland AM, Vredenbregt-van den Berg MS, Willemsen R, Luider T, Pasa-Tolic L, Jenster G. Proteomic profiling of exosomes leads to the identification of novel biomarkers for prostate cancer. PLoS One 2013; 8: e82589.

[23] Nicholson JK, Connelly J, Lindon JC, Holmes E. Metabonomics: a platform for studying drug toxicity and gene function. Nat Rev Drug Discov 2002; 1: 153-161.

[24] Roth S, Rottach A, Lotz-Havla AS, Laux V, Muschaweckh A, Gersting SW, Muntau AC, Hopfner KP, Jin L, Vanness K, Petrini JHJ, Drexler I, Leonhardt H, Ruland J. Rad50-CARD9 interactions link cytosolic DNA sensing to IL-1β production. Nat Immunol 2014; 15: 538-545.